High Frame Rate Echocardiography for Detailed Analysis of Cardiac Dynamics

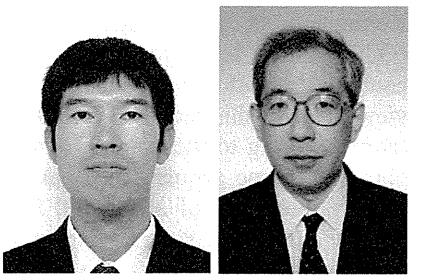

Hideyuki Hasegawa[1,2)] and Hiroshi Kanai[*2,1)]

Professor
1) Graduate School of Biomedical Engineering
2) Graduate School of Engineering
E-mail: hasegawa@ecei.tohoku.ac.jp, hkanai@ecei.tohoku.ac.jp

Abstract

Echocardiography is a widely-used modality for diagnosis of the heart. It enables observation of the shape of a heart and estimation of global heart function based on B-mode and M-mode imaging. Subsequently, methods for estimating myocardial strain and strain rate have been developed to evaluate regional heart function. Furthermore, it has been recently shown that measurements of transmural transition of myocardial contraction/relaxation and propagation of vibration caused by closure of a heart valve would be useful for evaluation of myocardial function and viscoelasticity. However, such measurements require a frame rate much higher than that achieved by conventional ultrasonic diagnostic equipment. In the present study, a method based on parallel receive beamforming was developed to achieve high-frame-rate echocardiography over 300 Hz. To increase the frame rate, the number of transmits was reduced to 15 with angular intervals of 6 degrees, and 16 receiving beams were created for each transmission to obtain the number and density of scan lines which were same as those realized by conventional sector scanning. In addition, several transmits were compounded to obtain each scan line to reduce the differences in transmit-receive sensitivities among scan lines. The number of transmits for compounding was determined by considering the width of the transmit beam. For transmission, plane waves and diverging waves were investigated. Diverging waves showed better performance than plane waves because the widths of plane waves did not increase with the range distance from an ultrasonic probe, whereas lateral intervals of scan lines increased with range distance. The spatial resolution of the proposed method was validated using fine nylon wires. Although the widths at half maxima of the point spread functions obtained by diverging waves were slightly larger than those obtained by conventional beamforming and parallel beamforming with plane waves, the point spread functions, which were very similar to that obtained by conventional beamforming could be realized by parallel beamforming with diverging beams and compounding. However, there was an increase in the lateral sidelobe level in the case of parallel beamforming with plane and diverging waves. Furthermore, a heart of a 23-year-old healthy male was measured. Although contrast of the B-mode image obtained by the proposed method was degraded due to the increased sidelobe level, a frame rate of 316 Hz, which was much higher than that realized by conventional sector scanning of several tens of Hertz, was realized with a full lateral field of view of 90 degrees.

1. Introduction

Echocardiography is one of the predominant modalities for the diagnosis of the heart because it provides a cross-sectional image of the heart noninvasively in real time. Owing to the high temporal resolution of ultrasonic diagnostic equipment, global heart function, such as ejection fraction (EF), can be estimated based on B-mode and M-mode imaging much more easily compared with other diagnostic modalities, such as magnetic resonance imaging (MRI) and computed tomography (CT). To evaluate regional myocardial function quantitatively, methods for measurements of myocardial strain and strain rate have been developed [1-3]. These methods enable estimation of regional deformation of the heart wall based on measurements of movement. Although measured strain and strain rate themselves are useful for evaluation of the regional myocardial function, it has recently been shown that the measurements of transmural transition of myocardial contraction/relaxation and propagation of vibration caused by closure of a heart valve would be useful for evaluation of myocardial function and viscoelasticity [4-6]. However, such measurements require a frame rate much higher than that achieved by conventional ultrasonic diagnostic equipment. For example, electrical excitation propagates in Purkinje fibers and ventricular muscle at typical velocities of 0.3 to 4 m/s [7], and the corresponding propagation velocities of myocardial contraction of 0.5 to 7 m/s were measured by ultrasound [5,8]. A high frame rate, typically higher than 200 Hz, which is much higher than that realized by conventional ultrasonic diagnostic equipment of several tens of Hertz, is required to measure the propagation of this electromechanical wave and the resulting transient small motion of the heart wall.

Konofagou et al. [9] and D'hooge et al.[10] increased the frame rate to above 200 Hz by reducing the size of the field of view and the total number of scan lines in an ultrasonic image. Furthermore,

Konofagou et al. introduced a electrocardiogram (ECG)-gating technique in ultrasound imaging to combine individual small sectors into a large field of view [11]. In this method, the lateral size of a sector (corresponding to the number of scan lines), which is obtained in one acquisition, is narrowed to achieve a higher frame rate of about 500 Hz. By measuring a number of small sectors during the corresponding number of cardiac cycles, the measured small sectors are combined into a large sector format based on ECG-gating. Although this method achieves a frame rate of about 500 Hz, which is much higher than the conventional frame rate of several tens of Hertz, measurements for a number of cardiac cycles are required.

To achieve a high frame rate of about 500 Hz without ECG-gating, we used sparse sector scanning, in which the number of scan lines was decreased to about 10 [12]. In this method, the angle intervals between scan lines are increased to obtain a large lateral field of view with a small number of scan lines. Therefore, the lateral image resolution is significantly degraded.

The above-mentioned methods are based on conventional beamforming. Therefore, they need to sacrifice the density of scan lines or field of view to achieve a high frame rate. To overcome this problem, parallel receive beamforming with a wide transmit beam have been developed13) to illuminate a wider region by one transmission to reduce the number of transmissions. This could be done in the cited study by conventional transmit beamforming (focusing at a certain range distance) because such beams are wide in the region shallower than the focal distance (between the transducer surface and the focal point). Using this method, real-time 3D imaging of the heart was realized at a frame rate of a few tens of Hertzes. However, the width of the transmit beam is narrower than the size of an aperture, and this would limit the number of receiving beams created by one transmission.

Lu et al. proposed an alternative imaging method using unfocused but non-diverging transmit beam, namely, limited diffraction beam [14-17]. Unfocused beams achieved a wider beam width, and non-diverging beams used in these cited studies prevent the insonified energy from being spread to assure the required penetration depth. However, the width of a non-diverging beam is still limited by the size of an aperture.

On the other hand, diverging beams have potential to enlarge the region illuminated by one transmission. In synthetic aperture ultrasound imaging, a single element or a small number of elements are used to produce spherical waves [21,22]. Although a spherical wave can illuminate a wide area by one transmission, acoustic pressure significantly decreases with propagation distance, and the signal-to-noise ratio (SNR) of the received signal would be significantly reduced.

In the present study, the feasibility of a diverging transmit beam in ultrasonic imaging with parallel beamforming [18-20] was investigated to achieve a frame rate above 200 Hz with an adequate lateral spatial resolution, a wider field of view, and no ECG-gating. Diverging waves can be produced by using all transducer elements in an ultrasonic array probe to obtain ultrasonic echoes with better SNR.23) The width of diverging angle was limited to suppress the decay of acoustic pressure due to the propagation distance. Furthermore, the diverging beam was steered to obtain an ultrasonic image of a heart with a full angle of 90 degrees with a limited beam width. To increase the frame rate, the number of transmits was reduced to 15 with a transmit angular interval of 6 degrees, and 16 receiving beams were created in each transmit to obtain the number and density of scan lines which were same as those realized by conventional sector scanning. The spatial resolution of the proposed imaging method was evaluated by basic experiments using fine nylon wires. Furthermore, B-mode images of a heart of a 23-year-old healthy male measured by the proposed method were obtained.

2. Materials and Methods

2.1. Mathematical description of ultrasound waves emitted from transducer elements

Let us describe ultrasound waves emitted from transducer elements of a phased array ultrasonic probe. To achieve a frame rate over 200 Hz under a typical pulse repetition frequency of 5 kHz (realized by the ultrasound system used in the present study under a setting of an observation range of 130 mm), the number of transmits should be less than 25. Therefore, in the present study, plane waves or diverging waves were transmitted in 15 directions $\{m\Theta\}$ ($m = -7, -6, \cdots, 0, 1, \cdots, 7$) with angular intervals of $\Theta = 6$ degrees. The ultrasonic wave $g_{i,m}(\mathbf{p}; t)$ at time t from the time of transmission, which is emitted from the i-th transducer element ($i = 0, 1, \cdots, L-1$) in the m-th transmission and insonifies to a spatial point p = (r, θ), as shown in Fig. 1, is expressed as follows:

$$g_{i,m}(\mathbf{p}; t) = s_i\left(t - \tau_{t,i,m}(\mathbf{p})\right), \quad (2.1)$$

where $s_i(t)$ is the impulse response of the i-th transducer element, and $\tau_{t,i,m}(\mathbf{p})$ is a time delay due to propagation of an ultrasonic wave from the i-th element to the spatial point $\mathbf{p}$. The time delay $\tau_{t,i,m}(\mathbf{p})$ of $g_{i,m}(\mathbf{p}; t)$ is given by

$$\tau_{t,i,m}(\mathbf{p}) = \frac{\sqrt{r^2\cos^2\theta + \left\{r\sin\theta - \left(i - \frac{L-1}{2}\right)\Delta x\right\}^2}}{c_0} + T_{\mathrm{TBF},i,m}, \quad (2.2)$$

where Δx and c_0 are the lateral pitch of transducer elements and speed of sound, respectively, and $T_{\mathrm{TBF},i}$ is the time delay applied to the i-th element by the transmit beamformer.

To emit a plane wave at the steering angle of $m\Theta$, $T_{\mathrm{TBF},i,m}$ should be given by

$$T_{TBF,i,m} = \begin{cases} \frac{i\cdot\Delta x\cdot\sin(m\Theta)}{c_0} & if\ m \geq 0, \\ \frac{(i-L+1)\cdot\Delta x\cdot\sin(m\Theta)}{c_0} & if\ m < 0. \end{cases} \quad (2.3)$$

($i = 0, 1, \ldots, L\text{-}1$)

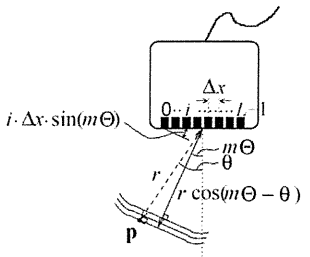

Fig. 1. Illustrations of a plane wave insonifying to spatial point **p** = (r, θ) and propagation distance r cos($m\Theta$ − θ) required to illuminate spatial point **p**, which is located at distance r from the center of array, using a plane wave.

The time delay $T_{\mathrm{TBF},i,m}$ applied by transmit beamformer is greater than or equal to zero.

For a circular planar transducer, the Fresnel zone (range of near field) is defined by the diameter of the aperture D and ultrasonic wavelength λ as $D^2/(4\lambda)$. The aperture width D of the sector probe and the ultrasonic wavelength λ used in the present study were about 20 mm and about 0.4 mm (center frequency: 3.75 MHz), respectively. Although the phased array probe used in the present study was not circular, the range of near field can be approximately obtained based on this equation. The range of the Fresnel zone of the probe used was 250 mm and, thus, the range of about 130 mm, which was imaged in the present study, was included in the near field. In the near field, the width of a plane wave is constant. On the other hand, in ultrasonic imaging in a sector format, the lateral width of a small sector imaged by one transmission increases with range distance and, thus, the performance of a plane wave would be limited because the lateral width of a plane wave does not increase with range distance in the near field.

To solve this problem, in the present study, a diverging wave, which is illustrated in Fig. 2(a), was used for transmission in addition to a plane wave. In synthetic aperture imaging, each single element is individually used to emit a spherical wave. Such diverging waves would be useful for ultrasonic imaging in a sector format. However, the intensity of the emitted wave would significantly decrease because a single element is used. Alternatively, spherically diverging waves [22] can be produced using all the transducer elements in every transmission. In the present study, such a diverging wave was realized by applying time delay $T_{\mathrm{TBF},i,m}$ to the i-th transducer element in the m-th transmission, which is given by

$$T_{\mathrm{TBF},i,m} = \begin{cases} \frac{i\cdot\Delta x\cdot\sin(m\Theta)}{c_0} + \frac{\sqrt{\left\{\left(i-\frac{L-1}{2}\Delta x\right)\right\}^2 + r_f{}^2} - r_f}{c_0} & if\ m \geq 0, \\ \frac{(i-L+1)\cdot\Delta x\cdot\sin(m\Theta)}{c_0} + \frac{\sqrt{\left\{\left(i-\frac{L-1}{2}\right)\right\}^2 + r_f{}^2} - r_f}{c_0} & if\ m < 0, \end{cases} \quad (2.4)$$

where r_f is the distance from a virtual point source Ov behind the array to the surface of the transducer array.

The first term in the right-hand side of eq. (2.4) is required to steer the direction of the transmit beam to $m\Theta$. The second term, which is required to realize a diverging wave, was obtained in the present study by considering the geometry illustrated in Fig. 2(b). The second term depends on the distance from the virtual point source O_v to the i-th element in Fig. 2(b).

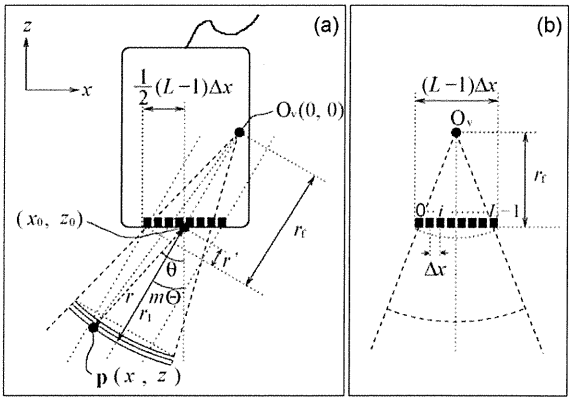

Fig. 2. Illustration of a diverging wave. (a) Propagation distance r1 required to illuminate spatial point p, which is located at distance r from the center of array, using a diverging wave. (b) Geometry for consideration of time delays applied to transducer elements for transmission of diverging wave.

2.2. Parallel receive beamforming

In this study, ultrasonic beams (plane or diverging waves) emitted in 15 directions an angle intervals of Θ = 6 degrees and 16 receiving beams with angle intervals of 0.375 degrees were created for each transmit to realize the number and density of scan lines which are similar to that obtained by conventional sector scanning. The value, $\hat{O}_m(\mathbf{p})$, of the beamformed RF signal at a spatial point **p** is generated from ultrasonic echo signals $\{y_{i,m}(t)\}$ received by the elements (i = 0, 1, ..., L − 1), which contain echoes scattered at all points illuminated by the m-th transmission, as follows:

$$\hat{O}_m(\mathbf{p}) = \sum_{i=0}^{L-1} w_{r,i}\cdot y_{i,m}\left(t - \tau_{\mathrm{RBF},i,m}(\mathbf{p})\right), \quad (2.5)$$

where $w_{r,i}$ (i = 0, 1, · · · , L − 1) corresponds to the receive apodization, and $\tau_{\mathrm{RBF},i,m}(\mathbf{p})$ is the time delay which should be applied by a receive beamformer to compensate the propagation delay of the emitted wave from the probe to **p** and that of the scattered wave from **p** to the i-th element. The time delay $\tau_{\mathrm{RBF},i,m}(\mathbf{p})$, which was applied by the receive beamformer to echo signal $y_{i,m}(t)$ received by the i-th element, is given by

$$\tau_{\mathrm{RBF},i,m}(\mathbf{p}) = T_{\mathrm{TW},m}(\mathbf{p}) + \frac{\sqrt{r^2\cos^2\theta + \left\{r\sin\theta - \Delta x\left(i-\frac{L-1}{2}\right)\right\}^2}}{c_0}. \quad (2.6)$$

The second term of eq. (2.6) corresponds to the time delay of a scattered echo from the spatial point p to the

i-th element. The first term, $T_{\mathrm{TW},m}(\mathbf{p})$, of eq. (2.6) corresponds to the propagation delay of the emitted ultrasonic wave to spatial point $\mathbf{p}$ which depends on the receiving beam angle θ. In the present study, as illustrated in Fig. 1, for a plane wave, $T_{\mathrm{TW},m}(\mathbf{p})$ was assigned as follows:

$$T_{\mathrm{TW},m}(\mathbf{p}) = \frac{r\cos(\theta - m\Theta)}{c_0}. \quad (2.7)$$

For diverging waves, as illustrated in Fig. 2(b), $T_{\mathrm{TW},m}(\mathbf{p})$ was assigned as follows:

$$T_{\mathrm{TW},m}(\mathbf{p}) = \frac{\sqrt{x^2+z^2} - r_f + r'}{c_0}, \quad (2.8)$$

$$x = r_f \sin(m\Theta) - r' \sin(m\Theta) + r\sin\theta, \quad (2.9)$$

$$z = -r_f \cos(m\Theta) + r' \cos(m\Theta) - r\cos\theta, \quad (2.10)$$

$$r' = \frac{1}{2} \cdot (L-1) \cdot \Delta x \cdot \sin(m\Theta), \quad (2.11)$$

where (x, z) is the position of $\mathbf{p}$ in the Cartesian coordinate.

By changing θ $((m-0.5)\cdot\Theta \leq \theta < (m+0.5)\cdot\Theta)$ at intervals of 0.375 degrees at each range position r in each of the m transmissions, beamformed RF signals $\{\hat{O}_m(\mathbf{p})\}$ at all spatial points $\{\mathbf{p} = (r, \theta)\}$ in the field of view are obtained.

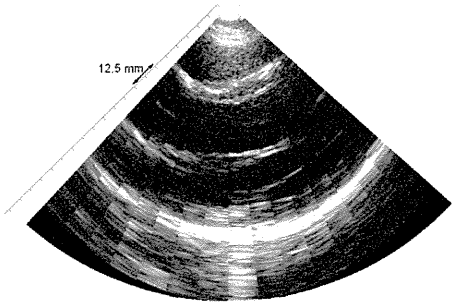

Fig. 3. Longitudinal B-mode image of a heart of a 23-year-old male obtained by parallel beamforming without spatial compounding.

2.3. Problem in parallel beamforming with phased array

To obtain an ultrasonic image in a sector format, ultrasonic beams need to be steered. Therefore, the directivity of the ultrasound beam changes depending on the steering angle. In receive beamforming, the difference between the directivities of neighboring receiving beams is not so significant because the angle intervals of receiving beams are small (0.375 degrees). However, such difference is significant in transmission because of a relatively large angle interval of neighboring transmit beams of 6 degrees (used in the present study). This significant change in directivity in transmission produce discontinuities in a resultant ultrasonic image at a pitch of 6 degrees, which corresponds to angular intervals of transmit beams because the transmit-receive directivity is defined by the product of the transmit and receive directivities [24]. Figure 3 shows a B-mode image of the heart of a 23-year-old healthy male, which was obtained using parallel beam forming expressed by eq. (2.5) with plane wave transmission. As can be seen in Fig. 3, there are significant discontinuities at the edges of each region imaged by one transmission.

2.3. Spatial compound of multiple transmits in receive beamforming

As described in the previous section, there are discontinuities in an ultrasound image when each scan line is created by each single transmission because the lateral intensity profiles of transmit beams significantly differ between transmissions due to a large angular interval of transmit beams (in general, the intensity is decreased by steering due to directivities of transducer elements). Such discontinuities consist of high spatial (angular) frequency components, which degrade the image quality. A simple way to reduce such discontinuities (high spatial frequency components) in an ultrasound image obtained by parallel beamforming is to use spatial moving average, i.e., low-pass filtering. Spatially averaged beamformed RF signal $\hat{O}_s(r, \theta)$ at a spatial point $\mathbf{p} = (r, \theta)$ is expressed as follows:

$$\begin{aligned}\hat{O}_s(r,\theta) &= \sum_{j=-M_s}^{M_s} w_j \cdot \hat{O}_{m0}(r, \theta + \Theta) \\ &= \sum_{j=-M_s}^{M_s} w_j \cdot \hat{O}_{m0}(r, \theta + \Theta \cdot j) \\ &\quad \cdot \exp\{-j2\pi f_\theta (\Theta \cdot j)\}|_{f_\theta = 0},\end{aligned} \quad (2.12)$$

where the number of averaging is expressed by $(2M_s + 1)$, w_j is a weighting function, and m_0 is the transmission number that gives the minimum difference between the direction of transmission $m\Theta$ and the direction θ of point $\mathbf{p} = (r, \theta)$. As can be seen in eq. (2.12), the moving average operation corresponds to the Fourier transform with respect to an angular frequency f_θ of zero. The spatial frequency spectrum obtained by eq. (2.12) is expressed by the convolution of the spatial frequency characteristics of w_j and $\hat{O}_m(r, \theta)$ and, thus, the spatial frequency characteristics of low-pass filtering by moving average operation is determined by that of the weighting function w_j. It is well known that a rectangular weighting function exhibits a higher sidelobe level in the frequency domain, which corresponds to higher leakage of high spatial frequency components. Therefore, a tapered function, such as a Hanning window, which exhibits lower sidelobe level, is preferable for weighting function w_j.

Although the high spatial frequency components can be reduced by spatial averaging, the image would be blurred because the beamformed RF signals $\{\hat{O}_m(\mathbf{p})\}$ at different spatial positions $\{\mathbf{p}\}$ are averaged in eq. (2.12). To avoid such blurring effect, in the present

study, RF signals $\{\hat{O}_m(\mathbf{p})\}$ beamformed with respect to the same spatial position $\mathbf{p}$ in different transmissions $\{m\}$ are compounded. This procedure has a similar effect given by eq. (2.12) because the lateral intensity profiles of unfocused beams, such as plane wave and diverging wave, are almost homogeneous at every angle θ within the beams. Therefore, we assumed that $\hat{O}_{m0}(r, \theta + \Theta \cdot j) \approx \hat{O}_{m0+j}(r, \theta)$.

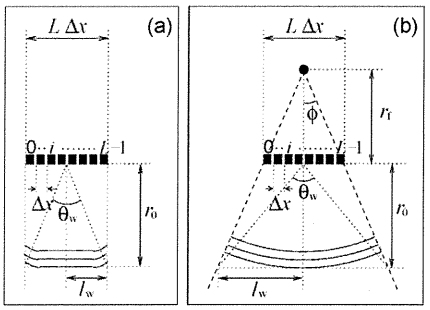

Fig. 4. Illustration of angular width θw of emitted wave. (a) Plane wave. (b) Diverging wave.

By replacing the summation with respect to angle in eq. (2.12) by that with respect to transmission, the compounded beamformed RF signal $\hat{O}_c(\mathbf{p})$ at $\mathbf{p}$ is expressed as follows:

$$\hat{O}_c(p) = \sum_{j=-M_c}^{M_c} w_{c,m0+j}(\mathbf{p}) \cdot \hat{O}_{m0+j}(\mathbf{p}), \qquad (2.13)$$

where the number of compounding is expressed as $(2M_c + 1)$. In the present study, Hanning weighting was used in spatial compounding and is expressed as follows:

$$w_{c,m}(p) = \cos^2\left\{\frac{\pi}{2} \cdot \frac{(\theta - m\Theta)}{\frac{1}{2} \cdot (2M_c + 1)\Theta}\right\}, \qquad (2.14)$$

where the number of compounding is expressed as $(2M_c + 1)$. In the present study, M_c was determined from the angular width of the emitted wave by considering the transducer geometry, as illustrated in Fig. 4. For plane waves, the angular width θ_w at range distance r is given by

$$\theta_w = 2\arctan\left(\frac{L \cdot \Delta x}{2r}\right). \qquad (2.15)$$

For diverging waves, the diverging angle φ is obtained as follows:

$$\varphi = \arctan\left(\frac{L \cdot \Delta x}{2r_f}\right). \qquad (2.16)$$

In the present study, using the diverging angle φ, the lateral beam width l_w at range distance r is approximately given by

$$l_w = (r_f + r)\tan\phi. \qquad (2.17)$$

The angular width θ_w for diverging wave is obtained as follows:

$$\theta_w = 2\arctan\frac{l_w}{r}. \qquad (2.18)$$

The number of compounding $(2M_c + 1)$ is determined so that the contribution of the emissions, whose directions are different from the direction of interest θ by larger than half the angular beam width θ_w, are gradually decreased. In the present study, this was given by $(2M_c + 1)\Theta/2 < \theta_w$. To satisfy this condition, the number of compounding was determined as follows:

$$M_c = \left\lfloor \frac{\theta_w}{\Theta} \right\rfloor. \qquad (2.19)$$

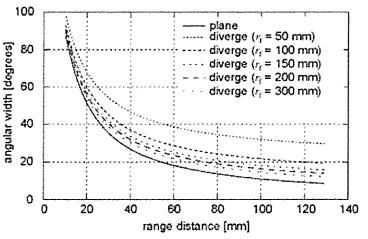

Fig. 5. Angular widths $\{\theta_w\}$ calculated for plane and diverging waves.

In the present study, the angular beam width θ_w were introduced to consider the relationship between the beam width and the interval of transmit beams because sparser transmissions requires a larger beam width to illuminate a larger region between the directions of successive transmissions. The angular beam width is more convenient than the beam width in distance because the angular interval of transmit beams does not change with the range distance, whereas the interval in distance changes. In Fig. 5, angular widths $\{\theta_w\}$ calculated for plane and diverging waves using eqs. (2.15) and (2.18) are plotted as functions of range distance r (size of aperture $L \cdot \Delta x$ = 19.2 mm was the same as that of the ultrasonic probe used). Angular width θ_w of a diverging wave at distance r_f of a virtual point source larger than 100 mm does not change so much compared with that of a plane wave. At the longest range distance of 130 mm, which was of interest in the present study, angular width θ_w doubles at r_f = 100 mm and triples at r_f = 50 mm. Angular width θ_w would further increase at smaller r_f. However, the intensity of the emitted wave would further decrease. Therefore, in the present study, diverging waves at r_f = 100 mm and 50 mm were investigated in the subsequent sections.

3. Results

3.1. Evaluation of spatial resolution using a wire phantom

In the present study, a commercial ultrasonic diagnostic system (α-10, Aloka, Tokyo, Japan) was used with a 3.75-MHz phased array probe. This system was modified so that RF echoes received by L = 96 individual elements could be acquired at a sampling frequency of 30 MHz for off-line processing (receive beamforming, spatial compounding, etc.).

In the basic experiment, fine nylon wires (diameter ≈ 100 μm) placed in water were used for evaluation of the spatial resolution. Figures 6(a)-(d) show B-mode

images of the wires obtained by conventional sector scanning and parallel beamforming with spatial compounding using plane waves and diverging waves at r_f = 100 mm and 50 mm, respectively. In Figs. 6(1) and 6(2), rectangular apodization ($w_{r,i}$ = 1; i = 0, 1, 2, ..., L − 1) and Hamming apodization ($w_{r,i}$ = 0.54−0.46 cos(2πi/L); i = 0, 1, 2, ..., L−1) were respectively used. As can be seen in Fig. 6, the sidelobe levels significantly increased when rectangular apodization was used. Therefore, Hamming apodization was used in the subsequent experiments.

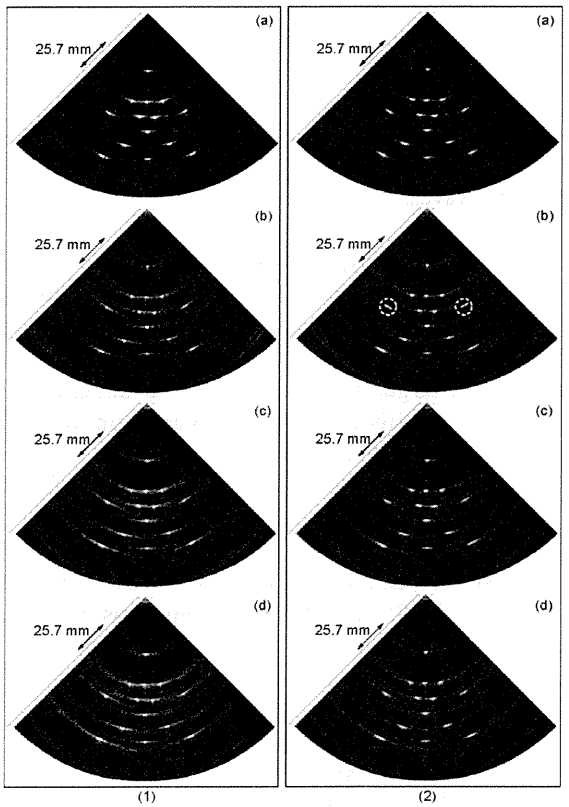

Fig. 6. B-mode images of fine wires obtained by (a) conventional sector scanning and parallel beamforming using (b) plane waves, (c) diverging waves at r_f = 100 mm, and (d) diverging waves at r_f = 50 mm. (1) Rectangular and (2) Hamming apodizations were used.

In the B-mode image obtained by parallel beamforming with plane waves, the point spread function at a larger steering angle (surrounded by white dashed lines in Fig. 6(2-b)) was distorted (split in the lateral direction) because the widths of plane waves were narrow compared with diverging waves and the widths decreased when the steering angle was increased. Therefore, the use of plane waves is limited to imaging at smaller steering angles. On the other hand, such distortion was not found in the B-mode images obtained by parallel beamforming with diverging waves.

Figures 7(a) and 7(b) show the axial and lateral profiles of the images (corresponding to point spread functions) at an angular position θ of 0 degrees and range distance r of 41 mm, respectively. The widths at half maxima of the point spread functions shown in Fig. 7 are described in table I. As shown in Fig. 7, plane wave transmission achieved the best lateral spatial resolution. Although the widths at half maxima of the point spread functions obtained by diverging waves were slightly larger than those obtained by conventional beamforming and parallel beamforming with plane waves, the point spread functions, which were very similar to that obtained by conventional beamforming could be realized by parallel beamforming with diverging beams and compounding. Figures 8(a) and 8(b) illustrate point spread functions created by compounding plane and diverging waves, respectively. The wavefronts and point spread functions shown by the dashed and solid lines illustrate those obtained by the transmission at the least steering angle and that at the maximum steering angle in beamforming with respect to spatial point **p**. The overlapping area of two point spread functions in Fig. 8 is enhanced in the resultant point spread function obtained by compounding. As can be seen in Fig. 8, the overlapping area obtained by plane waves is smaller than that obtained by diverging beams, even when the maximum steering angles are same. Therefore, it was considered that plane wave transmission achieved the best lateral spatial resolution. However, there was an increase of the lateral sidelobe level by use of parallel beamforming with both plane and diverging waves. Although this increase of the sidelobe level would degrade the image contrast, the lateral spatial resolution comparable to that of conventional sector scan was achieved by the proposed method.

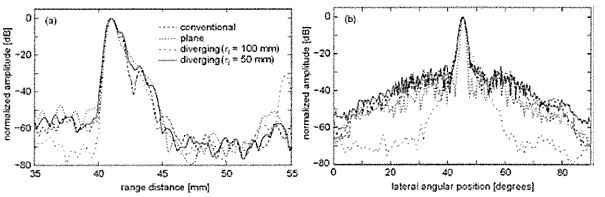

Fig. 7. Axial and lateral profiles of envelopes of beamformed RF echoes obtained by respective methods. (a) Axial profile at a lateral angular position of 0 degrees. (b) Lateral profile at a range distance of 41 mm.

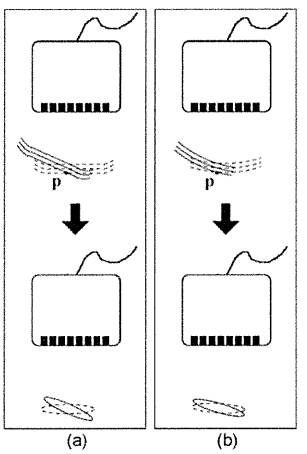

Fig. 8. Wavefronts and point spread functions produced by (a) plane waves and (b) diverging waves.

Table 1. Widths at half maxima of point spread functions shown in Fig. 7.

	conventional beamforming	plane wave	diverging wave (r_f = 100 mm)	diverging wave (r_f = 50 mm)
axial [mm]	0.73	0.71	0.88	0.84
lateral [mm]	0.68	0.52	0.81	0.86

In Fig. 7, the number of compounding ($2M_c + 1$) was determined by eq. (2.19). In Fig. 9(1) and 9(2), M_c was also determined by eq. (2.19), however, the maximum of M_c was limited to be 4 and 2, respectively. For diverging waves, B-mode images obtained by limiting the maximum number of compounding were better than those obtained with unlimited M_c, as shown in Fig. 6. In the present study, the propagation delay of the emitted wave was calculated based on eq. (2.8) without considering the distortion of wavefront due to beam steering. Therefore, it can be considered that the number of compounding M_c larger than 2 (corresponding to larger differences among the steering angles in emissions used for compounding) degraded the resultant images because it would be difficult to estimate propagation delays at larger steering angles by eq. (2.8) and the large number of transmissions (means a large difference among the angles of transmissions) used for compounding degrades coherent compounding. As in Fig. 7, Fig. 10 shows lateral profiles of envelopes of compounded beamformed RF echoes at a range distance of 41 mm obtained by a diverging beam at r_f = 50 mm with and without limitation of $M_c \leq 2$. In Fig. 10, only the profiles obtained with a diverging beam at r_f = 50 mm are shown because the number of compounding is largest among the transmit beams used in the present study. As shown in Fig. 10, degradation of coherent compounding reduces the difference between the main lobe and sidelobe levels and does not improve the spatial resolution. Consequently, in the present study, the number of compounding ($2M_c + 1$) was determined by eq. (2.19); however, its maximum was restricted to be 5 for diverging waves.

In general, the insonified energy of a diverging wave spreads and acoustic intensity decreases with propagation distance. To reduce this decay, in the present study, the width of the diverging beam was limited. Figure 11 shows the axial profiles of the ultrasound images of the wire phantom (shown in Fig. 6) at a lateral angle of 0 degrees. As expected, the intensity at the deepest wire was strongest when focusing was done in both transmit and receive, as shown in Fig. 11. Although the intensity was lower than that obtained by focusing in both transmit and receive, the diverging waves used in the present study achieved decays of intensities (Figs. 11(c) and 11(d)) which were similar to that realized by plane waves (Fig. 11(b)).

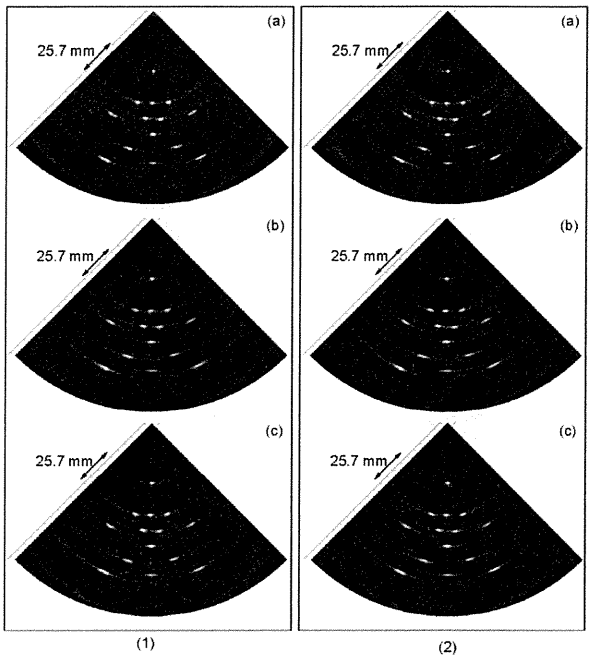

Fig. 9. B-mode images of fine wires obtained by parallel beamforming with (a) plane waves, (b) diverging waves at rf = 100 mm, and (c) diverging waves at rf = 50 mm. Maxima of the number of compounding were limited to be (1) 4 and (2) 2.

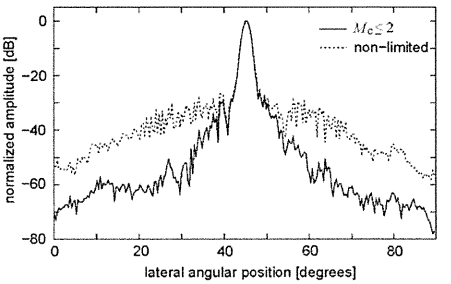

Fig. 10. Lateral profiles of envelopes of beamformed RF echoes at a range distance of 41 mm obtained by a diverging beam at r_f = 50 mm with and without limitation of $M_c \leq 2$.

3.2. *In Vivo* imaging of a human heart

Figure 12(a)-(d) shows B-mode images of the heart of a 23-year-old healthy male obtained by conventional sector scan and parallel beamforming with plane waves and diverging waves at r_f = 50 mm and 100 mm, respectively. The maximum of the number of compounding M_c was limited to 2 for diverging waves. Although a B-mode image of a heart could be obtained by plane wave transmission, the point spread function produced by parallel beamforming with plane waves were split in the lateral direction, as shown in Fig. 6. Therefore, it might be better to use plane wave transmission with a smaller maximum steering angle. By using diverging waves, as shown in Figs. 12(c) and 12(d), B-mode images of the heart could be obtained at a high frame rate of 316 Hz with a full lateral field of view of 90 degrees, and the diverging waves at r_f = 50

mm and 100 mm showed similar performances. Although the image contrast were degraded due to the higher lateral sidelobe levels, a B-mode image, whose image quality was comparable to that obtained by conventional sector scanning, could be obtained at a frame rate (316 Hz) significantly higher than that (39 Hz) obtained by conventional sector scan, and a full field of view of 90 degrees was achieved without requiring ECG gating [11].

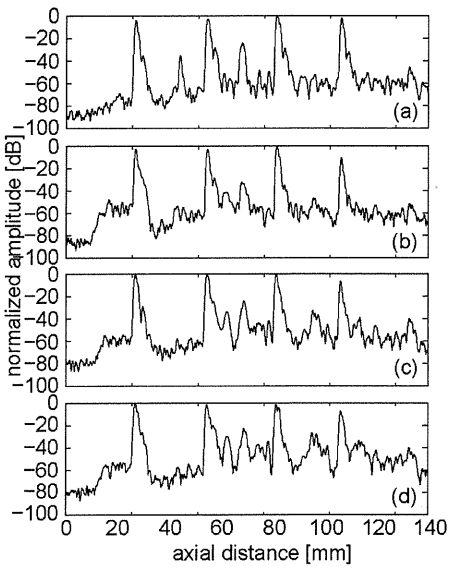

Fig. 11. Axial profiles of the images of wires (shown in Fig. 6) at a lateral angle of 0 degrees. (a) Conventional beamforming (focusing in both transmit and receive). (b) Parallel beamforming with plane waves. (c) and (d) Parallel beamforming with diverging beams at r_f = 100 mm and 50 mm, respectively.

4. Discussion

In the present study, a method based on parallel beamforming was investigated for high frame rate echocardiography. To realize B-mode imaging in a sector format based on parallel beamforming, spherically diverging waves were used in transmission.

In the present study, in receive beamforming, the propagation delay of the emitted diverging wave was calculated by considering the geometry of the transducer array and the virtual point source. However, the increase of the number of compounding M_c, which corresponds to the increase of the transmission steering angle from the direction of interest θ, degraded the resultant B-mode images. This would be caused by the distortion of the wavefront of the emitted wave due to steering. In future work, methods for accurate realization of the desired wavefront or accurate calculation of the resultant wavefront will be necessary to increase the number of compounding for further improvements of the image resolution because the difference in angles of wavefronts in different transmissions would increase by using more number of transmissions for compounding, as illustrated in Fig. 8. In addition, phase aberration correction [26,27] would be useful for receive beamforming.

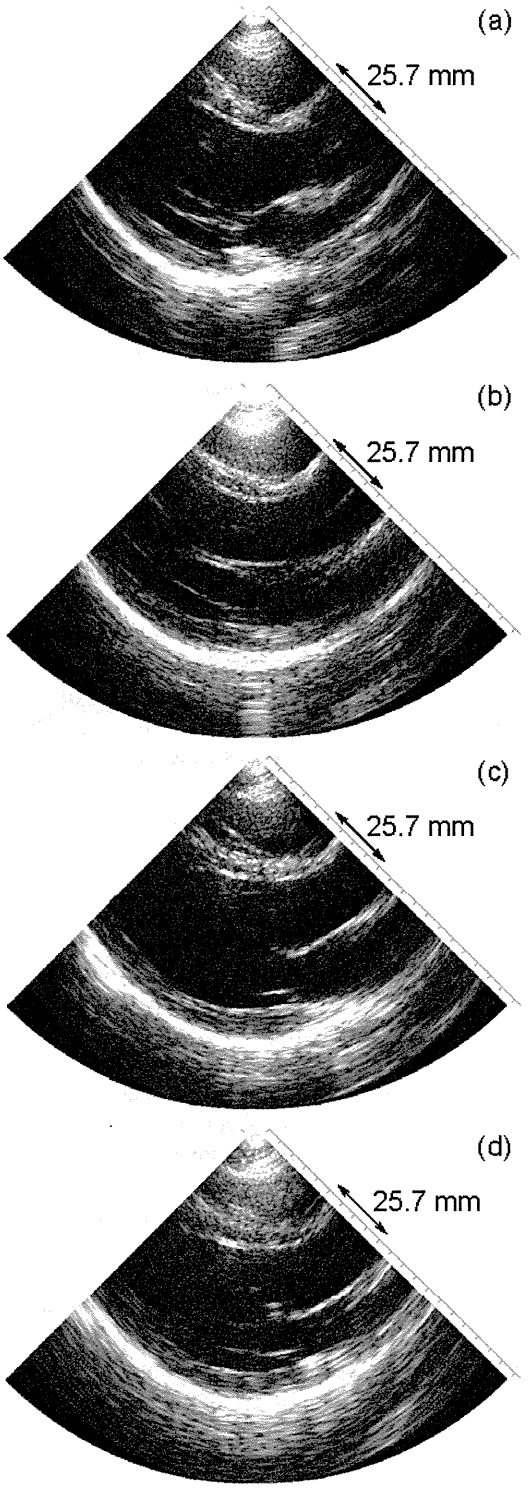

Fig. 12. B-mode images of a heart of a 23-year-old healthy male obtained by (a) conventional sector scanning and parallel beamforming using (b) plane waves, (c) diverging waves at rf = 100 mm, and (d) diverging waves at r_f = 50 mm. The maximum number of compounding was limited to be 2 for diverging waves.

Although diverging waves should be used to achieve a full lateral field of view of 90 degrees, plane waves could be used for imaging of a narrower region. Plane waves are more easily implemented in ultrasonic diagnostic equipment and make it easier to calculate the propagation delay of the wavefront. This was shown by the results in Fig. 9 that the increase of the maximum number of compounding did not degrade the resultant B-mode image in the case of plane wave transmission. The error in the calculated propagation delay at larger steering angles was considered to be smaller for plane waves than for diverging waves. Figure 13 shows a longitudinal B-mode image of the heart of the same subject as in Fig. 12 obtained with plane wave transmission and smaller steering angles. As can be seen in Fig. 13, a B-mode image of good quality can be obtained at a very high frame rate (1010 Hz) that is much higher than that (200 Hz) achieved by conventional sector scanning with a narrow field of view [10].

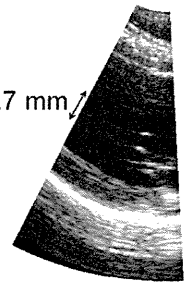

Fig. 13. B-mode image of the heart of the same subject as in Fig. 12 obtained by parallel beamforming with plane waves and a smaller maximum steering angle (frame rate: 1010 Hz).

The limitation of the current hardware used in the present study is that it takes about 1 minute to prepare for transmission of diverging waves. During this preparation, an operator needs to fix the position of the ultrasonic probe without viewing B-mode images. This limitation significantly increases the difficulties of in vivo measurements, particularly scanning of the same section several times. In future work, we need to develop a real-time system realizing the method proposed in the present study.

5. Conclusion

In this study, methods for measurement of viscoelasticity of arterial wall and evaluation of red blood cell aggregation were developed. Such methods would be useful for early diagnosis of atherosclerosis.

References

[1] Sutherland GR, Salvo GD, Claus P, *et al.* Strain and strain rate imaging: A new approach to quantifying regional myocardial function. *J Amer Soc Echocardiogr* **17**, 788-802, 2004.

[2] Sutherland GR, Stewart MJ, Groundstroem KW, *et al.* Color Doppler myocardial imaging: A new technique for the assessment of myocardial function. *J Amer Soc Echocardiogr* **7**, 441-458, 1994.

[3] Heimdal A, Støylen A, Torp H, *et al.* Real-time strain rate imaging of the left ventricle by ultrasound. *J Amer Soc Echocardiogr* **11**, 1013-1019, 1998.

[4] Yoshiara H, Hasegawa H, Kanai H, *et al.* Ultrasonic imaging of propagation of contraction and relaxation in the heart walls at high temporal resolution. *Jpn J Appl Phys* **46**, 4889-4896, 2007.

[5] Kanai H. Propagation of spontaneously actuated pulsive vibration in human heart wall and *in vivo* viscoelasticity estimation. *IEEE Trans Ultrason Ferroelectr Freq Control* **51**, 1931-1942, 2005.

[6] Kanai H. Propagation of vibration caused by electrical excitation in the normal human heart. *Ultrasound Med Biol* **35**, 936-948, 2009.

[7] Bers DM. *Excitation-contraction coupling and cardiac contractile force, 2nd ed.* Kluwer Academic Publishers, Dordrecht, 2001.

[8] Konofagou E, Luo J, Fujikura K, *et al.* Imaging the electromechanical wave imaging of cardiovascular tissue *in vivo*. In *Proc IEEE Ultrasonics Symp*, 985-988, 2006.

[9] Konofagou EE, D'hooge J, and Ophir J. Myocardial elastography–A feasibility study *in vivo*. *Ultrasound Med Biol* **28**, 475-482, 2002.

[10] D'hooge J, Konofagou E, Jamal F, *et al.* Two-dimensional ultrasonic strain rate measurement of the human heart *in vivo*. *IEEE Trans Ultrason Ferroelectr Freq Control* **49**, 281-286, 2002.

[11] Wang S, Lee W, Provost J, *et al.* A composite high-frame-rate system for clinical cardiovascular imaging. *IEEE Trans Ultrason Ferroelectr Freq Control* **55**, 2221-2233, 2008.

[12] Kanai H and Koiwa Y. Myocardial rapid velocity distribution. *Ultrasound Med Biol* **27**, 481-498, 2001.

[13] Bradley C. Retrospective transmit beamformation. *Whitepaper ACUSON SC2000TM Volume Imaging Ultrasound System*, 2008.

[14] Lu J. 2D and 3D high frame rate imaging with limited diffraction beams. *IEEE Trans Ultrason Ferroelectr Freq Control* **44**, 839-856, 1997.

[15] Lu J. Experimental study of high frame rate imaging with limited diffraction beams. *IEEE Trans Ultrason Ferroelectr Freq Control* **45**, 84-97, 1998.

[16] Cheng J and Lu J. Extended high-frame rate imaging method with limited-diffraction beams. *IEEE Trans Ultrason Ferroelectr Freq Control* **53**, 880-899, 2006.

[17] Lu J, Cheng J, and Wang J. High frame rate imaging system for limited diffraction array beam imaging with square-wave aperture weightings. *IEEE Trans Ultrason Ferroelectr Freq Control* **53**, 1796-1812, 2006.

[18] Shattuck DP, Weinshenker MD, and Smith SW. Explososcan: A parallel processing technique for high speed ultrasound imaging with linear phased arrays. *J Acoust Soc Amer* **75**, 1273-1282, 1984.

[19] Tanter M, Bercoff J, Sandrin L, *et al.* Ultrafast compound imaging for 2-D motion vector estimation:

Application to transient elastography. *IEEE Trans Ultrason Ferroelectr Freq Control* **49**, 1363-1374, 2002.
[20] Hasegawa H and Kanai H. Simultaneous imaging of artery-wall strain and blood flow by high frame rate acquisition of RF signals. *IEEE Trans Ultrason Ferroelectr Freq Control* **55**, 2626-2639, 2008.
[21] O'Donnell M and Thomas LJ. Efficient synthetic aperture imaging from a circular aperture with possible application to catheter-based imaging. *IEEE Trans Ultrason Ferroelectr Freq Control* **39**, 360-380, 1992.
[22] Karaman M and O'Donnell M. Synthetic aperture imaging for small scale systems. *IEEE Trans Ultrason Ferroelectr Freq Control* **42**, 429-442, 1995.
[23] Hasegawa H and Kanai H. Fast ultrasonic imaging of the heart using spherically diverging beam. *Technical Report of IEICE* **110**, 65-68, 2010.
[24] Mahafza BR. *Introduction to radar analysis*. CRC Press, Boca Raton, 1998.
[25] Jespersen SK, Wilhjelm JE, and Sillesen H. Multi-angle compound imaging. *Ultrason Imaging* **20**, 81-102, 1998.
[26] Fortes JMP. A closed loop ML algorithm for phase aberration correction n phased array imaging systems–Part I: Algorithm synthesis and experimental results. *IEEE Trans Ultrason Ferroelectr Freq Control* **44**, 259-270, 1997.
[27] Li Y. Phase aberration correction using near-field signal redundancy–Part I: Principles. *IEEE Trans Ultrason Ferroelectr Freq Control* **44**, 355-371, 1997.

RESEARCH REPORTS
Clinical

Y. Kobayashi, K. Niu*, L. Guan, H. Momma, H. Guo, Y. Cui, and R. Nagatomi*

Division of Biomedical Engineering for Health & Welfare, Tohoku University Graduate School of Biomedical Engineering, 2-1 Seiryo-machi, Aoba-ku, Sendai 980-8575, Japan; *corresponding authors, nkj0809@gmail.com and nagatomi@med.tohoku.ac.jp

J Dent Res 91(5):479-484, 2012

Oral Health Behavior and Metabolic Syndrome and Its Components in Adults

ABSTRACT

Inflammation has been strongly related to metabolic syndrome (MetS). Periodontal disease is the most common chronic infection in adults. We investigated a cross-sectional (n = 925) and 3-year longitudinal (n = 685) relationship between the daily frequency of toothbrushing and MetS. In the cross-sectional analysis, the prevalence of MetS was 15.7%. After adjustment for potential confounding factors (including all lifestyle factors), the odds ratios (95% confidence interval [CI]) of having MetS in those who brushed 2 times/day and ≥ 3 times/day were 0.71 (0.48-1.05) and 0.47 (0.24-0.92), respectively, as compared with ratios in those with a toothbrushing frequency of ≤ 1 time/day. Increasing toothbrushing frequency tended to relate inversely to hypertriglyceridemia and high-sensitivity C-reactive protein. In the longitudinal analysis, 99 participants were newly diagnosed with MetS. The adjusted odds ratios (95% CI) of the MetS in participants who brushed 2 times/day and ≥ 3 times/day as compared with participants who brushed ≤ 1 time/day were 0.80 (0.49-1.31) and 0.43 (0.19-0.97), respectively. The frequency of toothbrushing was related inversely only to hypertriglyceridemia, consistent with the cross-sectional analysis. This study found that more frequent toothbrushing is related to a lower prevalence and incidence of MetS. These results suggest that more frequent toothbrushing may contribute to the prevention of MetS due to the inflammation/triglyceride pathway.

KEY WORDS: toothbrushing, periodontal disease, cardiovascular risk factors, inflammatory, high-sensitivity C-reactive protein, CRP.

DOI: 10.1177/0022034512440707

Received September 16, 2011; Last revision January 31, 2012; Accepted February 1, 2012

INTRODUCTION

Metabolic syndrome (MetS) is a constellation of physiological and biochemical abnormalities characterized by disturbances of glucose metabolism, hypertension, dyslipidemia, and central obesity (Grundy, 2008). The prevalence of MetS has been increasing exponentially, and, in 2005, was reported to affect around 25% of the population in developed countries (Athyros *et al.*, 2005). The prevention of MetS is important, because it is a strong risk factor for cardiovascular disease (CVD) (Grundy *et al.*, 2005). Low-grade systemic inflammation is strongly related to an increased number of MetS components (Kirilmaz *et al.*, 2010).

Periodontal disease is a common chronic infection of the adult population, characterized by an exaggerated gingival inflammatory response against pathogenic bacterial microflora and resulting in alveolar bone and tooth loss (Williams, 1990). It is also related to low-grade inflammation (Slade *et al.*, 2000). Individuals with chronic periodontitis show a significant elevation in circulating inflammation-related factors (Ide *et al.*, 2004; Marcaccini *et al.*, 2009). Toothbrushing is effective in reducing the amount of bacterial plaque and gingivitis (Rimondini *et al.*, 2001), and toothbrushing that removes plaque from all tooth surfaces is essential to prevent the onset or development of inflammatory periodontal disease (Deery *et al.*, 2004; Ren *et al.*, 2007). Because low-level systemic inflammation is related to an increased risk of MetS (Lee and Pratley, 2005; Baranova, 2008), we hypothesized that more frequent toothbrushing might be related to MetS and its components.

Thus, we designed a cross-sectional study and a 3-year longitudinal study to investigate the relationship between the frequency of toothbrushing and the prevalence and incidence of MetS and its components in a Japanese adult population. To the best of our knowledge, this study is the first of its kind.

MATERIALS & METHODS

Study Population

The Oroshisho longitudinal study (from August 2008 to August 2011) was composed of a dynamic cohort of adult employees working at the Sendai Oroshisho Center, which is one group (over 120 enterprises) of small and medium enterprises (SME) in Sendai, northern Japan. Baseline data were obtained in August 2008. [A detailed description of the methods has been published elsewhere (Guo *et al.*, 2010).]

We used these baseline data in 2008 for cross-sectional analysis and 3-year follow-up data for longitudinal analysis. All individuals (n = 1,253) who received health examinations, which included blood tests, were invited to participate in this study. Of those, 1,154 agreed to participate and provided

informed consent for their data to be analyzed (response rate was 92.1%). Participants for whom toothbrushing information was unavailable (n = 89), those who used anti-hypertensive, lipid-lowering, or anti-diabetic agents (n = 135), and those with a history of CVD (n = 5) were excluded from the analysis. Thus, the final study population was comprised of 925 participants (696 men and 229 women). Of those invited, those who did not undergo health examinations in the follow-up period (n = 95) and those with MetS at baseline (n = 145) were excluded from longitudinal analysis. As a result, data from 685 participants were used in the longitudinal analysis (513 men and 172 women). The protocol for our study was approved by the Institutional Review Board of the Tohoku University Graduate School of Medicine. The study conforms to STROBE guidelines for cross-sectional and cohort studies.

Assessment of Oral Health Behavior

Self-reported frequency of toothbrushing *per* day in the preceding mo was assessed by a questionnaire, and participants were categorized into 3 groups: brushing teeth ≤ 1 time/day, 2 times/day, and ≥ 3 times/day.

Assessment of Metabolic Syndrome

Blood samples were drawn from the antecubital vein with minimal tourniquet use, with the participants in a seated position. Specimens were collected in siliconized vacuum glass tubes containing sodium fluoride for the analysis of fasting blood glucose (FBG) and no additives for lipid analysis. The FBG concentration was measured enzymatically (Eerotec Co., Ltd., Tokyo, Japan). The concentrations of triglycerides (TG), low-density lipoprotein cholesterol (LDL-C), and high-density lipoprotein cholesterol (HDL-C) were measured by enzymatic methods with appropriate kits (Sekisui Medical Co., Ltd., Tokyo, Japan). Blood pressure (BP) was measured twice from the upper left arm by means of an automatic device (Yamasu 605P; Kenzmedico, Saitama, Japan) after participants rested for 5 min in a sitting position, and the mean of the 2 measurements was taken as the BP value. Waist circumference (WC) was measured at the umbilical level with participants standing and breathing normally.

The criteria of the American Heart Association scientific statements of 2009 were used to define MetS (Alberti *et al.*, 2009). Participants were considered to have MetS if they presented with ≥ 3 of the following risk factors: (1) central obesity (WC ≥ 90 cm for men and ≥ 80 cm for women), (2) hypertriglyceridemia (TG ≥ 150 mg/dL), (3) low-HDL-C level (< 40 mg/dL for men and < 50 mg/dL for women), (4) high-BP (systolic ≥ 130 mm Hg or diastolic ≥ 85 mm Hg), and (5) high-FBG level (≥ 100 mg/dL).

Measurement of High-sensitivity C-reactive Protein (hsCRP)

Serum hsCRP concentrations were determined with N-latex CRP-2 (Siemens Healthcare Japan, Tokyo, Japan). The measurement limit of hsCRP was 0.02 mg/L, and an hsCRP value less than the measurement limit was considered to be 0.01 mg/L.

Assessment of Other Variables

The mean daily dietary intake was assessed according to a brief self-administered diet history questionnaire (Sasaki *et al.*, 2000) and calculated by means of an *ad hoc* computer program developed to analyze the questionnaire. Depressive symptoms were assessed according to the Japanese version of the Self-Rating Depression Scale (SDS) (Fukuda and Kobayashi, 1973). An SDS score of ≥ 40 was used as the cut-off point to indicate depressive symptoms (Barrett *et al.*, 1978). The participants' educational level was categorized as < college or ≥ college. The history of physical illnesses and current medications was also noted. Information on age, sex, smoking and drinking status, and occupation was obtained *via* a questionnaire survey. Levels of physical activity (PA) were estimated by the International Physical Activity Questionnaire (Craig *et al.*, 2003). Total weekly PA (metabolic equivalents [METs] × hrs/wk) was calculated (Craig *et al.*, 2003). PA was categorized into 2 groups based on a median PA level (PA ≥ 20 and PA < 20). The frequency of breakfast eating was assessed by the following question: "How many times do you eat breakfast a week?" and categorized into 2 groups of those eating breakfast < 4 times a week and those eating breakfast ≥ 5 times a week.

Statistical Analysis

Because the distribution of all continuous variables was not normal, the natural logarithm was applied to normalize the data before analysis. The continuous covariates after the log transformation neared normal distribution. To compare the participants' characteristics, we used the analysis of variance and the chi-squared test for continuous and categorical variables, respectively. Dichotomous variables were presented as percentages and continuous variables as the geometric mean (95% confidence interval [CI]). Multiple logistic regression analysis and analysis of covariance (ANCOVA) were used to analyze the relationship of the investigated parameters with MetS and MetS components as continuous variables, respectively. These analyses were performed after adjustment for potential confounding factors, including age, sex, smoking status, drinking status, breakfast eating, educational level, occupation (desk work or non-desk work), depressive symptoms, PA, and total caloric consumption (for MetS components analysis, additionally adjusted for mutual metabolic syndrome components individually). Interactions between the frequency of toothbrushing and potential confounders were tested by the addition of the cross-product terms in the regression model. For longitudinal analyses, multiple logistic regression analysis was used to examine the relationships between the frequency of toothbrushing and the incidence of MetS during the follow-up period after adjustment for potential confounding factors (see above). The reliability of the formative construct was performed by multicollinearity. Variance Inflation Factor (VIF) was used as an indicator for validity. VIF is less than 10, showing that no collinearity is accepted (Hair *et al.*, 2005). All statistical analyses were performed with SPSS version 17.0 (SPSS Japan Inc., Tokyo, Japan). All tests were 2-tailed, and $p < 0.05$ was considered statistically significant.

Table 1. Baseline Characteristics of the Participants in Relation to Frequency of Toothbrushing

Variable[a]	Frequency of Toothbrushing			p-value[b]
	≤ 1 Time/Day	2 Times/Day	≥ 3 Times/Day	
No. of participants (n = 925)	295	485	145	
Age (yrs)	45.0 (38.0-54.0)[c]	43.0 (36.0-53.0)	43.0 (36.0-54.0)	0.17
Male sex, no. (%)	262 (88.8)	359 (74.0)	75 (51.7)	< 0.001
Smoking status, no. (%)				
Never smoker	88 (29.8)	213 (43.9)	91 (62.8)	
Former smoker	33 (11.2)	63 (13.0)	15 (10.3)	
Current smoker	174 (59.0)	209 (43.1)	39 (26.9)	< 0.001
Drinking status, no. (%)				
Never drinker	69 (23.4)	101 (20.8)	39 (26.9)	
Occasional drinker	133 (45.1)	257 (53.0)	81 (55.9)	
Current drinker	93 (31.5)	127 (26.2)	25 (17.2)	< 0.05
SDS score ≥ 40, no. (%)	168 (56.9)	267 (55.1)	71 (49.0)	0.28
PA, ≥ 20 METs x hrs/wk, no. (%)	117 (39.7)	175 (36.1)	58 (40.0)	0.51
Educational level (≥ college), no. (%)	134 (45.4)	236 (48.7)	75 (51.7)	0.43
Occupation (desk work), no. (%)	110 (37.3)	215 (44.3)	93 (64.1)	< 0.001
Breakfast (≥ 5 times a wk), no. (%)	196 (66.4)	358 (73.8)	123 (84.8)	< 0.001
Daily dietary intake (kcal/d)	1814.1 (1471.7-2243.7)	1805.1 (1466.1-2191.3)	1791.9 (1373.7-2266.7)	0.93
Metabolic syndrome, no. (%)	62 (21.0)	70 (14.4)	13 (9.0)	< 0.01
Number of metabolic syndrome components	1.0 (1.0-2.0)	1.0 (0.0-2.0)	1.0 (0.0-2.0)	< 0.001
Waist circumference (cm)	84.0 (77.5-90.0)	81.0 (74.5-88.0)	78.0 (72.0-84.5)	< 0.001
SBP (mm Hg)	126.0 (116.0-138.0)	122.0 (112.0-135.0)	120.0 (110.0-130.0)	< 0.001
DBP (mm Hg)	80.0 (70.0-88.0)	78.0 (70.0-84.0)	76.0 (69.0-80.0)	< 0.001
HDL (mg/dL)	50.0 (42.0-59.0)	56.0 (46.0-66.0)	59.0 (50.0-69.0)	< 0.001
TG (mg/dL)	126.0 (83.0-189.0)	88.0 (64.5-136.5)	77.0 (49.5-116.0)	< 0.001
FBG (mg/dL)	94.0 (86.0-100.0)	90.0 (85.0-96.0)	90.0 (84.0-96.0)	< 0.001
hsCRP (mg/L)	0.40 (0.21-0.95)	0.29 (0.15-0.66)	0.22 (0.11-0.45)	< 0.001

[a]SDS, Self-rating Depression Scale; PA, physical activity; SBP, systolic blood pressure; DBP, diastolic blood pressure; HDL, high-density lipoprotein cholesterol; TG, triglyceride; FBG, fasting blood glucose; hsCRP, high-sensitivity C-reactive protein.
[b]ANOVA or χ^2 test.
[c]All values are medians; interquartile range in parentheses.

RESULTS

Of the 925 participants, 145 (15.7%) had 3 or more MetS components. Baseline characteristics of the participants in the different categories of toothbrushing are presented in Table 1. Among the more frequent brushing groups, there was a higher proportion of women, desk workers, those who usually ate breakfast, never smokers, and those who were occasional drinkers ($p < 0.05$), and a lower proportion of current drinkers and MetS ($p < 0.01$). Compared with participants who reported less frequent toothbrushing, those who frequently brushed their teeth had lower numbers of MetS components, WC, SBP, DBP, TG, FBG, and hsCRP levels and higher HDL-cholesterol levels ($p < 0.001$). No other significant differences were observed between the groups. The characteristics of the participants in the baseline and longitudinal analyses were similar, with the exception of the proportion of drinkers. No significant differences were observed between the categories of toothbrushing and drinking status ($p = 0.09$).

The prevalence of MetS was 21.0% (62/295) in those with a toothbrushing frequency of ≤ 1 time/day, 14.4% (70/485) in those who brushed 2 times/day, and 9.0% (13/145) in those who brushed ≥ 3 times/day. The Fig. shows the relationship between toothbrushing frequency and MetS (and its components) after adjustment for potential confounding factors. Adjusted odds ratios (OR, 95% CI) of MetS and hypertriglyceridemia in participants who brushed their teeth 2 times/day and ≥ 3 times/day as compared with participants who brushed ≤ 1 time/day were as follows: MetS, 0.71 (0.48-1.05) and 0.47 (0.24-0.92) (p for trend < 0.05); TG, 0.60 (0.41-0.86) and 0.45 (0.24-0.85) (p for trend < 0.01), respectively. No relationships were found between the categories of toothbrushing frequency and other MetS components.

The crude and adjusted relationships between the categories of toothbrushing frequency and the MetS components are shown in Table 2. In the final model, increasing toothbrushing frequency tended to relate inversely to triglycerides (p for trend < 0.05) and high-sensitivity C-reactive protein (p for trend < 0.01). The geometric means of the log-transformed TG related to toothbrushing ≥ 3 times/day were 11.1% lower as compared with those of toothbrushing ≤ 1 time/day (Bonferroni-corrected p-value < 0.05). Of all the covariants, sex, drinking status, and occupation were related to all MetS components, while smoking status was related to TG, HDL, and WC. The tests for interactions between the categories of toothbrushing frequency and these potential confounders in the final models were not found to be significant. Furthermore, the VIF levels of the multicollinearity of MetS components were as follows: TG, 1.40; FBG, 1.16; low HDL, 1.40; WC, 1.49; and SBP, 2.50, respectively.

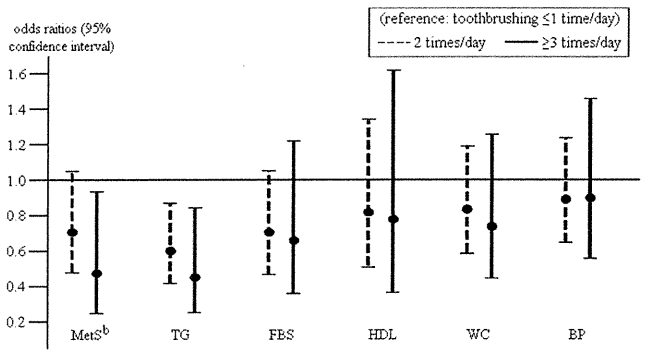

Figure. Adjusted odds ratio[a] (95% confidence interval) of the relationship between the categories of toothbrushing frequency and MetS and its components. [a]Adjusted for age, sex, smoking status, drinking status, breakfast status, educational level, occupation, depression status, physical activity, and total calories consumed *per* day (for MetS component analysis, additionally adjusted for mutual metabolic syndrome components individually). [b]MetS, metabolic syndrome; TG, triglyceride (≥ 150 mg/dL); FBG, fasting blood glucose (≥ 100 mg/dL); HDL, high-density lipoprotein cholesterol (< 40 for men / < 50 mg/dL for women); WC, waist circumference (≥ 90 cm for men / ≥ 80 cm for women); BP, blood pressure (systolic BP ≥ 130 or diastolic BP ≥ 85 mm Hg).

We evaluated the incidence of the MetS during a 3-year follow-up. During the follow-up periods, a total of 99 participants received a new diagnosis of MetS (incidence rate, 14.5%; 52 in 2009, 30 in 2010, and 17 in 2011). In the crude model, the OR (95% CI) of MetS in participants who brushed their teeth 2 times/day and ≥ 3 times/day, as compared with participants who brushed ≤ 1 time/day, were 0.63 (0.44-0.93) and 0.37 (0.20-0.70), respectively. In the final multivariate logistic models, the adjusted OR (95% CI) of MetS and hypertriglyceridemia in participants who brushed their teeth 2 times/day and ≥ 3 times/day, as compared with participants who brushed ≤ 1 time/day, were as follows: MetS, 0.80 (0.49-1.31) and 0.43 (0.19-0.97) (p for trend < 0.05); and hypertriglyceridemia, 0.63 (0.41-0.96) and 0.54 (0.27-1.05) (p for trend < 0.05), respectively. No relationships were found between the categories of toothbrushing frequency and other MetS components.

DISCUSSION

These cross-sectional and longitudinal studies investigated the relationship between toothbrushing and MetS (and its components). Our results suggest that more frequent toothbrushing is related to a lower prevalence and incidence of MetS.

We examined various potential confounders related to the frequency of daily toothbrushing, and found relationships between toothbrushing and 6 confounders, including gender, never smokers, occasional drinkers, current drinkers, occupation, and breakfast eating, which are similar to the results from previous studies (Dean *et al.*, 1992; Nakanishi *et al.*, 2005; Artnik *et al.*, 2008). The frequency of daily toothbrushing may be a marker for a healthier lifestyle. We found that the categories of toothbrushing frequency were related to several healthier lifestyle factors, including a lower proportion of current drinkers, and a higher proportion of those who ate breakfast and never smoked. However, the adjustment for these factors did not change the relationship between the categories of toothbrushing frequency and MetS (and its components). Previous studies have proposed that smoking is a major confounder in periodontal studies and is often an effect modifier (Hyman, 2006). However, there was no significant interaction between smoking and frequency of toothbrushing with MetS and its components, possibly due in part to the healthy population of participants.

In the final model, the frequency of toothbrushing was related inversely only to hypertriglyceridemia in both the cross-sectional and longitudinal analyses. Several studies have shown that, in periodontal disease, lipopolysaccharides derived from Gram-negative anaerobes trigger the production of tumor necrosis factor-alpha, a pro-inflammatory cytokine (Foster *et al.*, 2005; Tang *et al.*, 2006; Dornelles *et al.*, 2009) that plays a role in obesity and insulin resistance (Hotamisligil, 1999). Experimental studies in rats have also shown lipopolysaccharide administration to increase serum TG levels (Uchiumi *et al.*, 2004). Sepsis, an acute lipopolysaccharide-dependent pathological condition, has been shown to decrease the serum concentrations of total cholesterol, HDL-C, and apoproteins A and B, but to increase TG levels (Alvarez and Ramos, 1986). As suggested in these previous studies, inflammation, possibly mediated by lipopolysaccharides, may be strongly related to the serum level of lipid components, particularly TG. Toothbrushing is thought to improve gingivitis (Nathoo *et al.*, 2004), and in an experimental animal study, in addition to promoting the healing of periodontal lesions, it reduced serum lipopolysaccharide concentrations (Tomofuji *et al.*, 2009). Because the toothbrushing frequency in the cross-sectional study was related to hsCRP levels, which is a marker for inflammation, it is likely that frequent toothbrushing may have contributed to the reduction in TG *via* its effects on inflammation. The present results showed that the frequency of toothbrushing is related to MetS, mainly due to the inflammation/triglyceride pathway. Further study is needed to confirm these findings.

In a cohort study comprised of 11,869 community-dwelling adults, a higher toothbrushing frequency at baseline contributed to a lower risk of CVD events and a lower serum CRP concentration (de Oliveira *et al.*, 2010). Because increased MetS and its components are an independent risk factor for CVD events (Hokanson and Austin, 1996), our results suggest that the anti-inflammatory effect of toothbrushing may contribute to a reduction in CVD risk through the reduction in MetS risk. A longer follow-up study is necessary to confirm this hypothesis.

The present study has several limitations. Because we recruited the participants from those who had attended annual health check-ups within a limited time period, we could not examine their oral hygiene, particularly the actual prevalence of periodontal diseases. In addition, the frequency of toothbrushing was based on a self-reported questionnaire, in which no information was obtained regarding the time spent on each toothbrushing session. Moreover, because this was an observational study, we could not conclude whether the more frequent toothbrushing decreased MetS. Therefore, an intervention trial should be undertaken to confirm the existence of a relationship between toothbrushing frequency and MetS (and its components).

Table 2. Relationship between Toothbrushing Frequency and Metabolic Syndrome Components and hsCRP[a]

	Frequency of Toothbrushing			
	≤1 Time/Day (n = 295)	2 Times/Day (n = 485)	≥ 3 Times/Day (n = 145)	*p* for Trend[b]
Number of metabolic syndrome components				
Model 1[c]	1.6 (1.5-1.7)	1.4 (1.3-1.4)	1.3 (1.2-1.3)	< 0.001
Model 2[d]	1.5 (1.5-1.6)	1.4 (1.3-1.4)	1.3 (1.2-1.4)	< 0.001
Triglycerides (mg/dL)				
Model 1[c]	121.1 (113.3-129.5)[f]	94.7 (89.9-99.8)	78.7 (71.5-86.5)	< 0.001
Model 2[d]	111.2 (104.4-118.3)	95.7 (91.3-100.4)	90.4 (82.6-98.9)	< 0.001
Model 3[e]	105.7 (99.8-111.9)	97.5 (93.5-101.8)	94.0 (86.7-102.1)	< 0.05
Fasting blood glucose (mg/dL)				
Model 1[c]	94.5 (93.1-95.8)	91.5 (90.5-92.5)	90.5 (88.6-92.3)	< 0.01
Model 2[d]	93.8 (92.5-95.1)	91.6 (90.7-92.6)	91.4 (89.6-93.2)	< 0.05
Model 3[e]	93.3 (92.1-94.6)	91.8 (90.8-92.7)	91.8 (90.2-93.7)	0.23
HDL-cholesterol (mg/dL)				
Model 1[c]	50.3 (48.9-51.7)	55.6 (54.4-56.8)	58.3 (56.0-60.7)	< 0.001
Model 2[d]	51.8 (50.5-53.2)	55.5 (54.3-56.5)	55.6 (53.5-57.7)	< 0.01
Model 3[e]	53.0 (51.8-54.3)	55.0 (54.0-56.0)	54.3 (52.5-56.2)	0.26
Waist circumference (cm)				
Model 1[c]	83.4 (82.3-84.5)	81.1 (80.3-81.9)	78.2 (76.8-79.7)	< 0.001
Model 2[d]	82.6 (81.5-83.6)	81.1 (80.4-81.9)	79.8 (78.4-81.3)	< 0.01
Model 3[e]	81.5 (80.5-82.4)	81.5 (80.8-82.2)	80.5 (79.3-82.0)	0.32
Blood pressure (mm Hg)				
Systolic				
Model 1[c]	126.2 (124.3-128.0)	123.3 (121.9-124.8)	118.9 (116.5-121.5)	< 0.001
Model 2[d]	124.5 (122.8-126.2)	123.6 (122.3-124.8)	121.6 (119.2-124.0)	0.06
Model 3[e]	123.9 (122.1-125.4)	123.6 (122.5-125.0)	122.5 (120.2-124.8)	0.39
Diastolic				
Model 1[c]	78.7 (77.4-80.0)	76.7 (75.8-77.7)	73.8 (72.1-75.5)	< 0.001
Model 2[d]	77.6 (76.5-78.9)	76.9 (75.9-77.7)	75.3 (73.7-77.1)	< 0.05
Model 3[e]	77.1 (75.9-78.2)	76.9 (76.2-77.9)	76.0 (74.5-77.7)	0.37
hsCRP (mg/L)				
Model 1[c]	0.66 (0.57-0.76)	0.54 (0.48-0.61)	0.35 (0.25-0.47)	< 0.001
Model 2[d]	0.63 (0.53-0.72)	0.55 (0.49-0.62)	0.40 (0.29-0.52)	< 0.01

[a]hsCRP, high-sensitivity C-reactive protein; HDL, high-density lipoprotein.
[b]Analysis of covariance.
[c]Crude model.
[d]Adjusted for age, sex, smoking status, drinking status, breakfast status, educational level, occupation, depressive symptoms, physical activity, and total calories consumed *per* day.
[e]Additionally adjusted for mutual metabolic syndrome components.
[f]Adjusted geometric mean (95% confidence interval) (all such values).

Finally, since this study included only SME workers, these results might not represent 'big enterprise' workers' status.

In conclusion, our study found toothbrushing to be related to a lower prevalence and incidence of MetS as well as lower levels of its components, particularly TG. These results suggest that a simple daily maneuver may contribute to the prevention of MetS due to the inflammation/triglyceride pathway.

ACKNOWLEDGMENTS

The authors wish to thank the study participants and everyone from the Sendai Oroshisho Center who cooperated with the study. This study was funded by a Grant-in-Aid for "Knowledge Cluster Initiative" from the Ministry of Education, Culture, Sports, Science and Technology of Japan. The authors declare no potential conflicts of interest with respect to the authorship and/or publication of this article.

REFERENCES

Alberti KG, Eckel RH, Grundy SM, Zimmet PZ, Cleeman JI, Donato KA, *et al.* (2009). Harmonizing the metabolic syndrome: a joint interim statement of the International Diabetes Federation Task Force on Epidemiology and Prevention; National Heart, Lung, and Blood Institute; American Heart Association; World Heart Federation; International Atherosclerosis Society; and International Association for the Study of Obesity. *Circulation* 120:1640-1645.

Alvarez C, Ramos A (1986). Lipids, lipoproteins, and apoproteins in serum during infection. *Clin Chem* 32(1 Pt 1):142-145.

Artnik B, Premik M, Zaletel-Kragelj L (2008). Population groups at high risk for poor oral self care: the basis for oral health promotion. *Int J Public Health* 53:195-203.

Athyros VG, Ganotakis ES, Elisaf M, Mikhailidis DP (2005). The prevalence of the metabolic syndrome using the National Cholesterol Educational Program and International Diabetes Federation definitions. *Curr Med Res Opin* 21:1157-1159.

Baranova AV (2008). Adipokine genetics: unbalanced protein secretion by human adipose tissue as a cause of the metabolic syndrome. *Genetika* 44:1338-1355 [article in Russian].

Barrett J, Hurst MW, DiScala C, Rose RM (1978). Prevalence of depression over a 12-month period in a nonpatient population. *Arch Gen Psychiatry* 35:741-744.

Craig CL, Marshall AL, Sjostrom M, Bauman AE, Booth ML, Ainsworth BE, *et al.* (2003). International physical activity questionnaire: 12-country reliability and validity. *Med Sci Sports Exerc* 35:1381-1395.

de Oliveira C, Watt R, Hamer M (2010). Toothbrushing, inflammation, and risk of cardiovascular disease: results from Scottish Health Survey. *BMJ* 340:c2451.

Dean DH, Beeson LD, Cannon DF, Plunkett CB (1992). Condition of toothbrushes in use: correlation with behavioral and socio-economic factors. *Clin Prev Dent* 14:14-18.

Deery C, Heanue M, Deacon S, Robinson PG, Walmsley AD, Worthington H, *et al.* (2004). The effectiveness of manual versus powered toothbrushes for dental health: a systematic review. *J Dent* 32:197-211.

Dornelles FN, Santos DS, Van Dyke TE, Calixto JB, Batista EL Jr, Campos MM (2009). In vivo up-regulation of kinin B1 receptors after treatment with *Porphyromonas gingivalis* lipopolysaccharide in rat paw. *J Pharmacol Exp Ther* 330:756-763.

Foster N, Cheetham J, Taylor JJ, Preshaw PM (2005). VIP inhibits *Porphyromonas gingivalis* LPS-induced immune responses in human monocytes. *J Dent Res* 84:999-1004.

Fukuda K, Kobayashi S (1973). A study on a self-rating depression scale. *Seishin Shinkeigaku Zasshi* 75:673-679 [article in Japanese].

Grundy SM (2008). Metabolic syndrome pandemic. *Arterioscler Thromb Vasc Biol* 28:629-636.

Grundy SM, Cleeman JI, Daniels SR, Donato KA, Eckel RH, Franklin BA, *et al.* (2005). Diagnosis and management of the metabolic syndrome: an American Heart Association/National Heart, Lung, and Blood Institute Scientific Statement. *Circulation* 112:2735-2752; *erratum* in *Circulation* 112:e297-e298, 2005.

Guo H, Niu K, Monma H, Kobayashi Y, Guan L, Sato M, *et al.* (2010). Association of Japanese dietary pattern with serum adiponectin concentration in Japanese adult men. *Nutr Metab Cardiovasc Dis*:doi:10.1016/j.numecd.2010.1006.1006. [Epub ahead of print Sept 27, 2010].

Hair JF, Black W, Babin B, Anderson RE, Tatham RL (2005). Multivariate data analysis. 6th edition. New York, NY: Prentice-Hall, p. 230.

Hokanson JE, Austin MA (1996). Plasma triglyceride level is a risk factor for cardiovascular disease independent of high-density lipoprotein cholesterol level: a meta-analysis of population-based prospective studies. *J Cardiovasc Risk* 3:213-219.

Hotamisligil GS (1999). The role of TNFalpha and TNF receptors in obesity and insulin resistance. *J Intern Med* 245:621-625.

Hyman J (2006). The importance of assessing confounding and effect modification in research involving periodontal disease and systemic diseases. *J Clin Periodontol* 33:102-103.

Ide M, Jagdev D, Coward PY, Crook M, Barclay GR, Wilson RF (2004). The short-term effects of treatment of chronic periodontitis on circulating levels of endotoxin, C-reactive protein, tumor necrosis factor-alpha, and interleukin-6. *J Periodontol* 75:420-428.

Kirilmaz B, Asgun F, Alioglu E, Ercan E, Tengiz I, Turk U, *et al.* (2010). High inflammatory activity related to the number of metabolic syndrome components. *J Clin Hypertens (Greenwich)* 12:136-144.

Lee YH, Pratley RE (2005). The evolving role of inflammation in obesity and the metabolic syndrome. *Curr Diab Rep* 5:70-75.

Marcaccini AM, Meschiari CA, Sorgi CA, Saraiva MC, de Souza AM, Faccioli LH, *et al.* (2009). Circulating interleukin-6 and high-sensitivity C-reactive protein decrease after periodontal therapy in otherwise healthy subjects. *J Periodontol* 80:594-602.

Nakanishi N, Takatorige T, Suzuki K (2005). Cigarette smoking and the risk of the metabolic syndrome in middle-aged Japanese male office workers. *Ind Health* 43:295-301.

Nathoo S, Chaknis P, Petrone M, DeVizio W, Volpe AR (2004). A clinical comparison of the gingivitis reduction and plaque-removal efficacy of a new manual toothbrush. *Compend Contin Educ Dent* 25(10 Suppl 2):37S-45S.

Ren YF, Cacciato R, Whelehan MT, Ning L, Malmstrom HS (2007). Effects of toothbrushes with tapered and cross angled soft bristle design on dental plaque and gingival inflammation: a randomized and controlled clinical trial. *J Dent* 35:614-622.

Rimondini L, Zolfanelli B, Bernardi F, Bez C (2001). Self-preventive oral behavior in an Italian university student population. *J Clin Periodontol* 28:207-211.

Sasaki S, Ushio F, Amano K, Morihara M, Todoriki O, Uehara Y, *et al.* (2000). Serum biomarker-based validation of a self-administered diet history questionnaire for Japanese subjects. *J Nutr Sci Vitaminol (Tokyo)* 46:285-296.

Slade GD, Offenbacher S, Beck JD, Heiss G, Pankow JS (2000). Acute-phase inflammatory response to periodontal disease in the US population. *J Dent Res* 79:49-57.

Tang X, Metzger D, Leeman S, Amar S (2006). LPS-induced TNF-alpha factor (LITAF)-deficient mice express reduced LPS-induced cytokine: evidence for LITAF-dependent LPS signaling pathways. *Proc Natl Acad Sci USA* 103:13777-13782; published *erratum* in *Proc Natl Acad Sci USA* 104:315, 2007.

Tomofuji T, Ekuni D, Sanbe T, Azuma T, Tamaki N, Irie K, *et al.* (2009). Effects of improvement in periodontal inflammation by toothbrushing on serum lipopolysaccharide concentration and liver injury in rats. *Acta Odontol Scand* March 2009:1-6. [Epub ahead of print].

Uchiumi D, Kobayashi M, Tachikawa T, Hasegawa K (2004). Subcutaneous and continuous administration of lipopolysaccharide increases serum levels of triglyceride and monocyte chemoattractant protein-1 in rats. *J Periodontal Res* 39:120-128.

Williams RC (1990). Periodontal disease. *N Engl J Med* 322:373-382.

J Artif Organs (2012) 15:49–56
DOI 10.1007/s10047-011-0609-1

ORIGINAL ARTICLE

Engineering analysis of the effects of bulging sinuses in a newly designed pediatric pulmonary heart valve on hemodynamic function

Ichiro Suzuki · Yasuyuki Shiraishi · Shota Yabe · Yusuke Tsuboko · Telma Keiko Sugai · Ken Matsue · Takeyoshi Kameyama · Yoshifumi Saijo · Takashi Tanaka · Yoshihiro Okamoto · Zhonggang Feng · Takako Miyazaki · Masaaki Yamagishi · Makoto Yoshizawa · Mitsuo Umezu · Tomoyuki Yambe

Received: 7 February 2011 / Accepted: 6 September 2011 / Published online: 29 September 2011

Abstract The purpose of this study was to examine the hemodynamic characteristics of expanded polytetrafluoroethylene (ePTFE) pulmonary valves with bulging sinuses quantitatively in a pediatric pulmonary mechanical circulatory system designed by us, in order to propose the optimal design for clinical applications. In this study, we developed a pediatric pulmonary mock circulation system, which consisted of a pneumatic right ventricular model, a pulmonary heart valve chamber, and a pulmonary elastic compliance tubing with resistive units. The hemodynamic characteristics of four different types of ePTFE valves and a monoleaflet mechanical heart valve were examined. Relationships between the leaflet movements and fluid characteristics were evaluated based on engineering analyses using echocardiography and a high-speed video camera under the pediatric circulatory conditions of the mock system. We successfully performed hemodynamic simulations in our pediatric pulmonary circulatory system that could be useful for quantitatively evaluating the pediatric heart valves. In the simulation study, the ePTFE valve with bulging sinuses exhibited a large eddy in the vicinity of the leaflets, whereas the straight tubing exhibited turbulent flow. The Reynolds number obtained in the valve with bulging sinuses was calculated to be 1667, which was smaller than that in the straight tubing ($R_e = 2454$).

The hemodynamic characteristics of ePTFE pediatric pulmonary heart valves were examined in our mock circulatory system. The presence of the bulging sinuses in the pulmonary heart valve decreased the hydrodynamic energy loss and increased the systolic opening area. Based on an in vitro experiment, we were able to propose an optimal selection of pulmonary valve design parameters that could yield a more sophisticated pediatric ePTFE valve shape.

Keywords Pediatric pulmonary heart valve · ePTFE · Hemodynamic examination · Bulging sinus

I. Suzuki (✉) · S. Yabe · Y. Tsuboko · T. K. Sugai · Y. Saijo · M. Yoshizawa
Graduate School of Biomedical Engineering, Tohoku University, 4-1 Seiryo-machi, Aoba-ku, Sendai, Miyagi, Japan
e-mail: ichiro-rifle@pop02.odn.ne.jp

Y. Shiraishi (✉) · K. Matsue · T. Kameyama · T. Yambe
Institute of Development, Aging and Cancer, Tohoku University, 4-1 Seiryo-machi, Aoba-ku, Sendai, Miyagi, Japan
e-mail: shiraishi@idac.tohoku.ac.jp

T. Tanaka · Y. Okamoto · M. Umezu
Waseda University TWIns, Tokyo, Japan

Z. Feng
Department of Bio-System Engineering, Yamagata University, Yonezewa, Japan

T. Miyazaki · M. Yamagishi
Department of Pediatric Cardiovascular Surgery, Kyoto Prefectural University of Medicine, Kyoto, Japan

Introduction

Congenital cardiac malformations, such as tetralogy of Fallot and transposition of the great arteries, often result in right heart failure, which may require right ventricular outflow tract (RVOT) reconstruction. In these cases, it is necessary to reduce pulmonary arterial valve regurgitation [1–5].

The incidence of calcification in porcine bioprostheses and autologous pericardia is higher in children than in adults, which results in the poor durability of such valves in pediatric applications [6–14]. In order to reduce the generation of calcification, alternative materials such as ePTFE have been used in the fabrication of artificial valves.

Recently, the ePTFE valve with bulging sinuses shown in Fig. 1 has been applied to RVOT reconstruction. Yamagishi et al. [15, 16] reported RVOT reconstruction with the ePTFE valve with bulging sinuses in 325 patients from 2001 to 2011, none of whom had redo surgery due to valve malfunction related to calcification.

This excellent result motivated further attempts to improve the design and fabrication process of the ePTFE valves. However, there was a lack of information on the hemodynamic parameters associated with the mechanical structures involved in the design of the valve [17, 18]. The hypothesis of this study is that a vortex flow is generated in the vicinity of the bulging sinuses that results in optimal opening and closing of the leaflets. In this study, we developed a newly designed mechanical pulmonary circulatory system that facilitates the hemodynamic analysis of these artificial valves under the hydrodynamic conditions found in pediatric pulmonary circulation, and evaluated the hydrodynamic effects of the bulging sinuses on valve function.

Materials and methods

Valves employed

The valves examined in this study were as follows:

1. Monoleaflet mechanical heart valve (Björk–Shiley Monostrut)
2. Trileaflet ePTFE valve with bulging sinuses

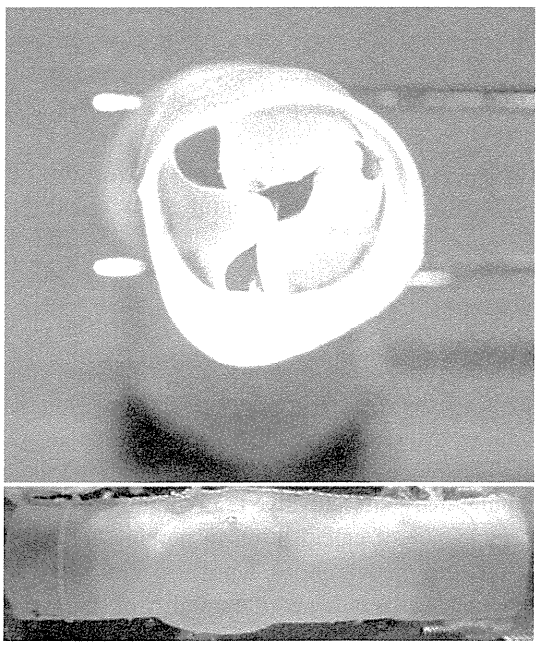

Fig. 1 Frontal and lateral views of an ePTFE valve with a bulging sinus

3. Trileaflet ePTFE valve in straight tubing without bulging sinuses

We employed a Björk–Shiley Monostrut valve for the mechanical settings of the mock circulatory system.

In the ePTFE valves, the conduit diameter and the thickness were 18 and 0.1 mm, respectively. To construct the bulging sinuses, an ePTFE sheet (thickness of 0.6 mm) was heated over a negative pressure in a vacuum pump, forcing it to fit to a mold of dome-shaped bulging sinuses. The cusps and these bulging sinuses were sutured along the conduit wall. In the conduits without bulging sinuses, the leaflets were sutured to the wall in the same area. There were two leaflet variations: fan-shaped and unfan-shaped.

The valved conduit with fan-shaped leaflets was fabricated with straight suture lines (S1) and curved bottom suture lines (S2), as shown in Fig. 2. The conduit with unfan-shaped leaflets was designed to allow a comparison of the effect of shape, and had straight suture lines (S1) and a point of suture (S3). A folded sheet was used to fabricate the valved conduit with unfan-shaped leaflets.

The two conduits were then compared.

We compared the effect of leaflet shape as well as the effect of bulging sinuses on the valvular characteristics. Figure 2 shows the four configurations analyzed in this study: (1) a valved conduit with bulging sinuses, B(+), and fan-shaped leaflets, F(+); (2) a straight valved conduit without bulging sinuses, B(−), and fan-shaped leaflets, F(+); (3) a valved conduit with bulging sinuses, B(+), and unfan-shaped leaflets, F(−); (4) a straight valved conduit without bulging sinuses, B(−), and unfan-shaped leaflets, F(−).

Pediatric pulmonary mock circulatory system

We developed a newly designed pediatric mechanical pulmonary circulatory system for the evaluation of valve function, as shown in Figs. 3 and 4. The system consisted of a right ventricular model, a valve chamber, an observation window, a reservoir tank, and a pulmonary arterial model with resistive units. The right ventricular model consisted of a cone-shaped silicone sac. The inflow portion of the right ventricular model was connected to the elastic right atrial rubber tubing. The valve to be evaluated was mounted in the valve chamber. The pulmonary arterial model was fabricated from silicone rubber. The resistance of the pulmonary arterial model was controlled by the resistive unit attached to the pulmonary arterial model.

Pulsatile flow was generated by a pneumatic artificial heart driver. Water at room temperature was used as the circulating medium. A bileaflet polymer valve was installed between the ventricle and the atrial model. These mechanical components were placed on the experimental table, and the mean inlet pressure of the ventricular model

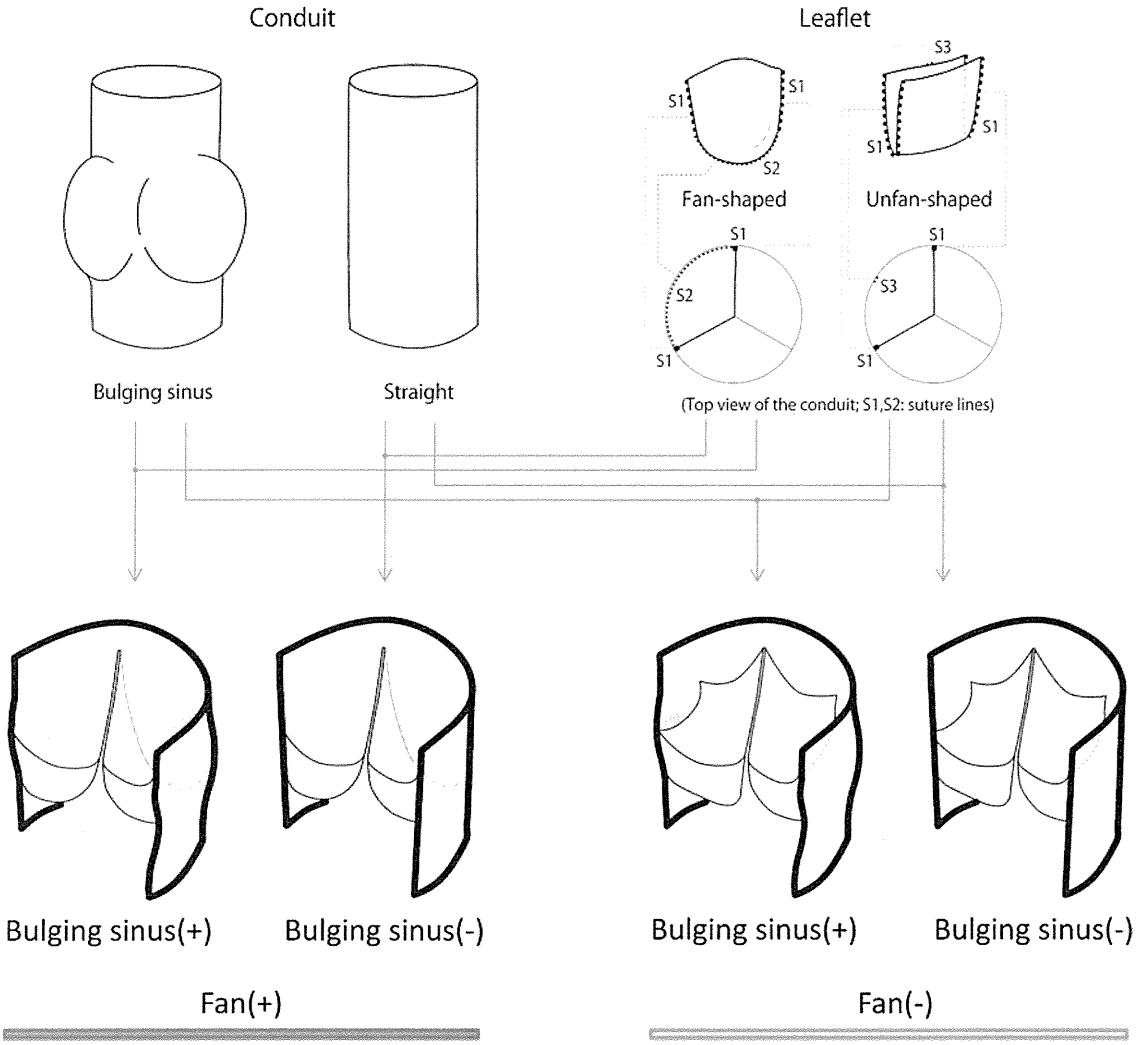

Fig. 2 The four configurations of ePTFE valves that were evaluated in this study: with or without bulging sinuses, and with unfan-shaped or fan-shaped leaflets

was set to be 5 mmHg by the reservoir tank head, which was capable of simulating natural central venous pressure. The pulmonary arterial pressure was controlled by the resistive unit representing pulmonary peripheral resistance. The mean pulmonary arterial pressure was set to be 15 mmHg with the Björk–Shiley valve as a control circulatory condition. The settings of the mechanical parameters were fixed throughout the study to examine variations in valve function.

Pulmonary valve test

Prior to the measurements, the ePTFE valves were immersed in silicone oil under vacuum pressure to ensure that it permeated into the ePTFE. An ultrasonic blood flow probe (Transonic Systems, TS410) was connected between the pulmonary valve and the ventricle. The transmural pressure of the valve was measured with two pressure transducers and recorded simultaneously at a sampling frequency of 500 Hz. The movements of the leaflets were captured through the observation window by a high-speed video camera (CASIO, EX-F1) at 300 fps. Each valve opening area was calculated through binarization from the digitally recorded sequential data (National Instruments, Labview Motion). These valve movements were recorded by synchronizing with the control for the pneumatic pump driver. The pulmonary valve chamber was filled with deaerated water. We investigated the flow velocity through the valve leaflets using an ultrasound system (HP, Sonos5000) [19, 20].

The ventricular model was driven at 60 and 120 bpm. The mean flow rate was set to 0.7 l/min with a positive

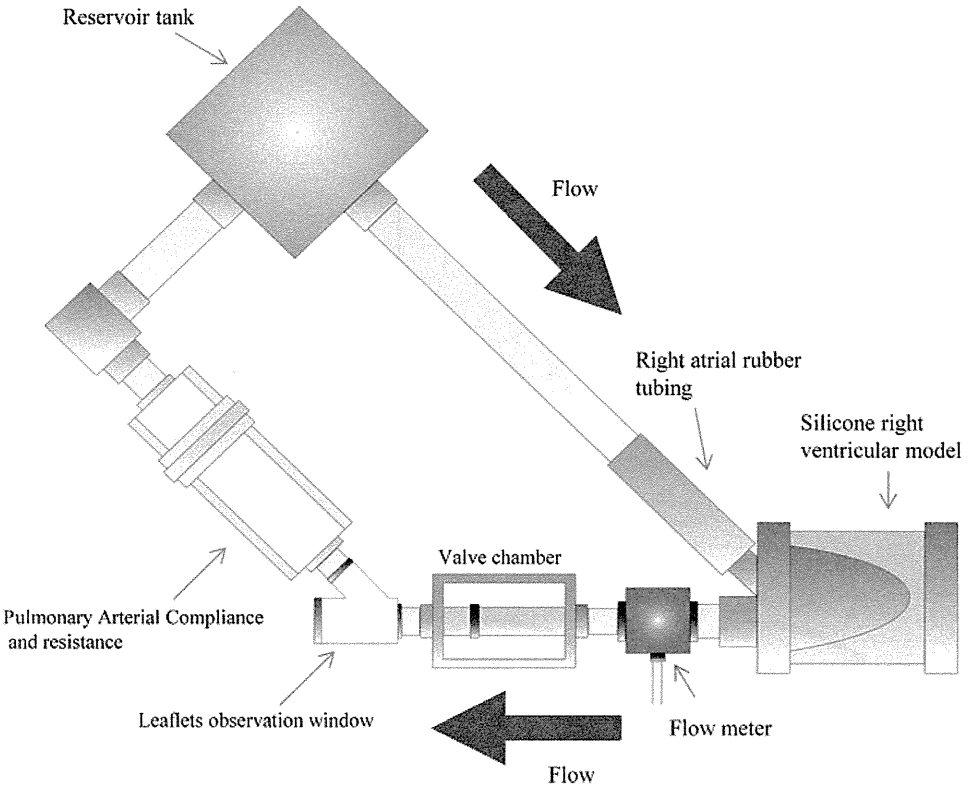

Fig. 3 Pediatric pulmonary mock circulatory system

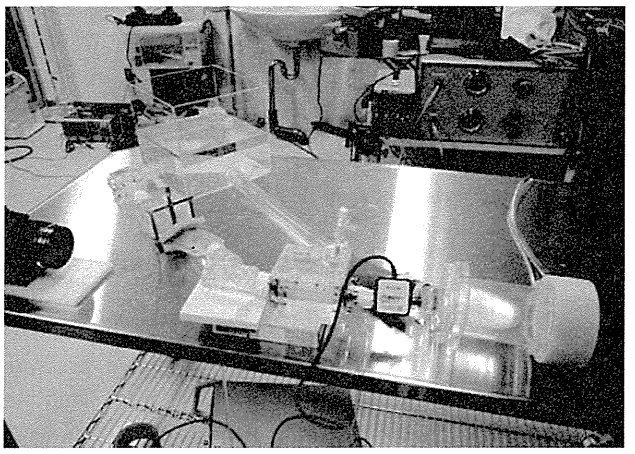

Fig. 4 Picture of the developed pediatric pulmonary mock circulatory system

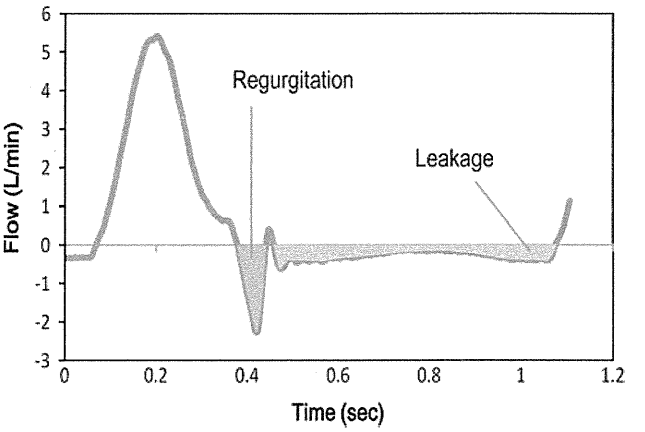

Fig. 5 Reverse-flow indicators for the evaluation of prosthetic valve function

driving pressure of 20 mmHg and a negative pressure of −5 mmHg throughout this examination, using the mono leaflet valve as a control.

Regurgitant flow (defined in Fig. 5) was obtained for each valve in the mock system. We examined the energy loss (as defined in Eq. 1) and calculated the opening area based on the pictures captured sequentially by the high-speed video camera [21].

$$E_{\text{loss}} = \int_{q>0} \Delta p(t) \cdot q(t) \mathrm{d}t, \tag{1}$$

where E_{loss} is the transvalvular energy loss, Δp is the transvalvular pressure gradient, and q is the flow.

In order to evaluate the hydrodynamic characteristics of each valve, we calculated the effective orifice area (Eq. 2) [22]. We also evaluated the flow characteristics using the